The Astrophysical Journal, 683:375–382, 2008 August 10

SPH SIMULATIONS OF DIRECT IMPACT ACCRETION IN THE ULTRACOMPACT AM CVn BINARIES

Joshua Dolence,[1] Matt A. Wood, and Isaac Silver
Department of Physics and Space Sciences and SARA Observatory, Florida Institute of Technology, Melbourne, FL 32901;
dolence2@astro.uiuc.edu, wood@fit.edu, isilver@fit.edu
Received 2006 October 24; accepted 2008 May 2

ABSTRACT

The ultracompact binary systems V407 Vul (RX J1914.4+2456) and HM Cnc (RX J0806.3+1527), a two-member subclass of the AM CVn stars, continue to generate interest because they defy unambiguous classification. Three proposed models remain viable at this time, but none of the three are significantly more compelling than the remaining two, and all three can satisfy the observational constraints if parameters in the models are tuned. One of the three proposed models is the direct impact model of Marsh & Steeghs, in which the accretion stream impacts the surface of a rapidly rotating primary white dwarf directly, but at a near-glancing angle. One requirement of this model is that the accretion stream have a high enough density to advect its specific kinetic energy below the photosphere for progressively more thermalized emission downstream, a constraint that requires an accretion spot size of $\sim 1.2 \times 10^5$ km^2 or smaller. Because we had at hand a smoothed particle hydrodynamics code optimized for cataclysmic variable accretion disk simulations, it was relatively straightforward for us to adapt it to calculate the footprint of the accretion stream at the nominal radius of the primary white dwarf and thus to test this constraint of the direct impact model. We find that the mass flux at the impact spot can be approximated by a bivariate Gaussian with a standard deviation of $\sigma_\phi = 164$ km in the orbital plane and $\sigma_\theta = 23$ km in the perpendicular direction. The area of the $2\,\sigma$ ellipse into which $\sim$86% of the mass flux occurs is roughly 47,400 km^2, or roughly half the size estimated by Marsh & Steeghs. We discuss the necessary parameters of a simple model of the luminosity distribution in the postimpact emission region.

Subject headings: accretion, accretion disks — binaries: general — hydrodynamics — novae, cataclysmic variables — stars: individual (RX J1914.4+2456) — white dwarfs — X-rays: binaries — X-rays: stars

1. INTRODUCTION

Understanding the exact physical nature of the ultracompact binaries (UCBs) V407 Vul (RX J1914.4+2456) and HM Cnc (RX J0806.3+1527) has been the goal of extensive studies ever since these two closely related systems were discovered. The observational results tightly constrain the universe of possible solutions (Cropper et al. 2004; Barros et al. 2007):

1. The "on/off" X-ray light curves folded on phase look nearly identical for the two systems, rising steeply to maximum, declining by half over the width of the pulse, and then dropping steeply again to zero.
2. The single observed and so presumed orbital periods are 321.5 s (5.36 minutes) for HM Cnc (Motch & Haberl 1995; Cropper et al. 1998; Ramsay et al. 2002) and 569.4 s (9.49 minutes) for V407 Vul (Ramsay et al. 2000; Steeghs et al. 2006).
3. The observed periods are decreasing with time (Strohmayer 2002; Hakala et al. 2003; Strohmayer 2004; Ramsay et al. 2005, 2006), consistent with the rate predicted for angular momentum losses by gravitational radiation.
4. There is an apparent phase difference in the optical and X-ray light curves in both systems in which the optical light curves lead the X-ray light curves by $\sim$0.2 in phase (Barros et al. 2007).
5. No hard X-rays are detected.
6. There is long-term variability in the mean luminosities of the systems (Israel et al. 1999; Ramsay et al. 2002; Israel et al. 2002).
7. Flickering, if present in the optical light curves, is of small amplitude, which suggests that the optical light is not dominated by radiation coming directly from the accreting region (Barros et al. 2007).

Of the several models proposed to explain the early observations of these systems, three remain viable at this time: (1) the polar model, (2) the direct impact (DI) model, and (3) the unipolar inductor (UI) model. In all three of the currently viable models, both the primary and secondary stars are thought to be white dwarf stars, but only for the polar and DI models does the secondary fill its Roche lobe. Each of the three can explain the observations with varying degrees of success, but some fine tuning is required, and in the case of the UI model the physical process is unfamiliar and unproven in a stellar context.

Historically, the system V407 Vul was discovered first and was suggested to be a double degenerate "soft" intermediate polar (IP) with a white dwarf spin period of 568 s (Motch & Haberl 1995). Cropper et al. (1998) noted that no other known IP displayed *zero* X-ray luminosity for $\sim$1/2 the observed period, and they proposed that the system was instead a double degenerate analog of the polars. HM Cnc was identified in the following year (Israel et al. 1999; Beuermann et al. 1999), and in 2002 two separate groups suggested independently that this system is a near-twin of V407 Vul (Ramsay et al. 2002; Israel et al. 2002). In contrast, the binary ES Cet, with an orbital period of 10.3 minutes, only slightly longer than that of 9.5 minutes for V407 Vul, shows clear signs of an accretion disk and is a typical AM CVn binary (Warner & Woudt 2002; Cropper et al. 2004). The IP model is unlikely to apply to these systems, in that the pulse shape of the X-ray light curve, the lack of hard X-rays and emission lines, and the infrared colors that seemingly exclude a main-sequence secondary are all difficult to explain within the IP model (Cropper et al. 2004). We do not discuss this model further, but the interested reader may wish to consult Norton et al. (2004).

[1] Current address: Department of Astronomy, University of Illinois at Urbana-Champaign, Urbana, IL 61801.

The polar model for the V407 Vul stars proposes that a Roche lobe–filling secondary transfers He-rich plasma to the magnetized and synchronized primary star, where it is channeled by the magnetic field onto the nearest magnetic pole, which is fixed in the corotating frame. Orbital motions take the accretion spot and column in and out of view, producing the X-ray light curves. The phase-offset optical variations are thought to arise from reprocessing on the face of the secondary star. Problems with this model include that emission lines and polarization are common in polars but are not observed here, and that mass transfer from a lower mass secondary to a higher mass primary should increase the orbital period. In regards to this last point, however, two separate groups (Deloye & Taam 2006; D'Antona et al. 2006) have shown that secondaries that are still contracting and nondegenerate can yield decreasing orbital periods while the mass transfer is in its early phases, and they can exist in this state for 10^3–10^6 yr. This is sufficient time for them to fulfill the requirements of observed space densities based on population synthesis models (Nelemans et al. 2001).

The DI model proposes that the two stars are close enough that the accretion stream impacts the surface of the primary white dwarf directly (Marsh & Steeghs 2002) because the stellar radius is larger than the "periastron" of a ballistic stream originating at the inner Lagrange point L1. Marsh & Steeghs (2002) argue that in the DI model, the accretion stream will be sufficiently narrow (with a width of $\sim 10^{-4}\ R_\odot$) that the density of the accreted material will be high enough to penetrate below the photosphere and thermalize to soft X-rays, similar to the blob accretion model proposed for some polars (Kuijpers & Pringle 1982; Frank et al. 1988; King 2000). For this to apply in the DI model, the surface area of the accretion spot must be a fraction of $f \sim 10^{-4}$ of the surface area of the star or smaller, which translates to an area smaller than $\sim 1.2 \times 10^5$ km^2. The initial motivation for this project came from P. Hakala, who suggested to one of us (M. W.) that it would be useful to use our smoothed particle hydrodynamics (SPH) code to accurately determine the accretion spot size. If a hydrodynamic simulation were to find that the footprint of the accretion stream is substantially larger than the Marsh & Steeghs (2002) estimate, then that would be a serious problem for the DI model. Of course, it is a one-sided test, and passing the test does not mean that the DI model is correct, only that it is consistent with the physical constraints of the blob accretion model.

The unipolar inductor (UI) model proposed by Wu et al. (2002) and discussed most recently in the context of V407 Vul and HM Cnc by Dall'Osso et al. (2006, 2007) and Ramsay et al. (2007) is the stellar analog of behavior observed in the Jupiter-Io system. As Io moves through Jupiter's magnetic field, charge separation occurs, and because the environment is a weak plasma, an EMF is established from the far point of Io as observed from Jupiter, along the magnetic field lines in both directions to Jupiter's atmosphere in both hemispheres, and from the planet back to the near side of Io (Goldreich & Lynden-Bell 1969). Resistive heating resulting from the current flow in the region between the two spots in each pair makes these regions luminous, as was observed by the *Hubble Space Telescope* (Clarke et al. 1996). Wu et al. (2002) suggested that this model, scaled to HM Cnc and V407 Vul, could explain the observations: certainly a fascinating and clever idea, even if it was eventually determined not to be applicable to these stars.

In a stellar context, the rate of energy dissipation in the UI model can be of order $L_\odot$ or higher, and with the predicted hot spot area of $\sim 8 \times 10^4$ km^2, the Wu et al. (2002) model predicts a 50 eV temperature, which is consistent with the 55 eV temperature observed from *ROSAT* and *ASCA* spectral fits (Ramsay et al. 2000). The hot spots are on the plane that passes through both the line of centers and the orbital rotation axis, and the source of the optical light modulation is again assumed to be reprocessed radiation from the heated face of the secondary. An important point in this model is that the secondary does not fill its Roche lobe, and there is no significant mass transfer. To first order, the timescale for orbital evolution is that which gravitational radiation predicts, consistent with the observed rates of the period change (Strohmayer 2002; Hakala et al. 2003; Strohmayer 2004; Ramsay et al. 2005, 2006). Ramsay et al. (2007) note that the UI model predicts radio emission, which they detected at the 5.8 σ level along the line of sight to HM Cnc, but which was not detected in observations of V407 Vul. The major problem with this model is the phasing of the optical versus X-ray light curves. Because the X-ray spots are on the meridian facing the secondary, this model predicts a phase offset of $\sim$0.5, whereas the observed phase offset is $\sim$0.2 for both V407 Vul and HM Cnc (Barros et al. 2007). In addition, Marsh & Nelemans (2005) suggest that there are serious problems with the synchronization timescales, but Dall'Osso et al. (2007) argue that the Marsh & Nelemans result rests on an estimate of the luminosity of V407 Vul that is too high by a factor of $\sim 10^2$. However, for the UI model to explain both systems, Dall'Osso et al. (2007) find that the primary white dwarf in HM Cnc rotates nearly synchronously but slightly slower than the orbital period, whereas the primary in V407 Vul must have a rotation frequency that is roughly 10% higher than the orbital frequency. The authors do not suggest how prior binary evolution without mass transfer can yield such a rapidly rotating primary.

In all three of the models above, the on/off behavior of the X-ray light curve has been interpreted to mean that the X-rays must be emitted from a geometrically compact region (Cropper et al. 1998, 2004). For the UI model, this region is the footprint of the magnetic field lines that carry current from the secondary (nonmagnetic) star to the primary (magnetic) star. Barros et al. (2005) analyzed this model and were able to place strict constraints on the allowable parameter space on the basis of geometrical arguments involving the size of this footprint. Here we present the results of a hydrodynamic simulation of V407 Vul that we made to estimate the area of the footprint of the accretion stream, in order to determine if the calculated spot size is small enough to satisfy the DI model requirement. In § 2 we discuss the changes that we made to our SPH code FITDisk in order to pursue this project, as well as the system parameters that we assumed. In § 3 we discuss the characteristics of the simulated accretion stream, and in § 4 we present our primary results. In § 5 we discuss our results in the context of the existing literature on V407 Vul and HM Cnc, and in § 6 we present our conclusions.

2. NUMERICS

2.1. *The Code*

We use the method of smoothed particle hydrodynamics, a Lagrangian-based technique that is well suited for astrophysical problems with unusual geometries and vacuum outer boundary conditions (Lucy 1977; Monaghan 1992, 2005). Our code FITDisk was developed to model accretion disks in cataclysmic variables (Simpson 1995; Simpson & Wood 1998; Wood et al. 2005, 2006; Wood & Burke 2007), and the details of the numerics can be found in those publications. In brief, FITDisk solves in the inertial frame the equations of compressible, viscous hydrodynamics, subject to the external gravitational field of two point-mass stars. Particles all have the same effective radius (smoothing length h) but can have different time step sizes as dictated by local conditions.

In our typical simulation runs, we build up a disk by injecting ~2000 particles per orbit at the L1 point until we reach the target number of particles in a particular run (~10^5). A particle is considered to be *accreted* onto M_1 when it is closer than the specified radius of the star. When this occurs (or accretion onto M_2, or ejection from the system), a replacement particle is immediately injected at the L1 point. Thus, the simulation in time settles into a dynamical equilibrium state.

Our goal with the current project is to test the requirement of the DI model of Marsh & Steeghs (2002) that the accretion spot on the surface of M_1 have an area of $A \lesssim 1.2 \times 10^5$ km^2, such that the stream density is sufficient to advect and release the stream kinetic energy below the photosphere, which is required in order to avoid hard X-ray emission. For this preliminary test, then, our main requirement is that the accretion stream behave as a fluid from the L1 region to the surface of the primary. We keep track of where the trajectories of the simulation particles intersect the mathematical surface of the primary and use the resulting integrated mass-flux distribution to estimate the effective area of the accretion spot. Our goal here is not to model in detail the hydrodynamics of the impact region; we are only beginning to address that far more ambitious calculation, and it will be the topic of a future publication. Our current results can be considered to provide the minimum estimated effective area for the accretion spot, as all physical effects that we have neglected could only act to increase the effective area.

To explore this problem, we made two substantial changes to our base code. First, we converted the code to make the calculations in the corotating frame instead of the inertial frame used in FITDisk up to this point, and second, we implemented a new particle injection scheme that gives a far more physical model of the flow dynamics through the inner Lagrange point L1.

Our original code performs calculations in the inertial frame, which generally simplifies the analysis and visualization steps, but for this project the analysis is simplified if the calculations are completed in the corotating frame with the implementation of Coriolis forces. We establish a Cartesian system, with the center of mass at the origin. The x-axis is along the line of centers of the two stars, with the donor star orbiting in the $+y$ direction and the orbital angular momentum vector in the $+z$ direction. Within this system, the stars, stream, and impact spot are stationary features. Therefore, the approximate point of impact for a given particle can be easily calculated by linear interpolation along its trajectory between its positions at the time steps t^{n-1} and t^n bracketing the primary surface radius. Also, in a steady state it becomes meaningful to examine the cumulative distribution of the particle mass flux as a function of position on the surface of the primary as a means to estimate the effective accretion spot size.

The mass transfer stream is created ab initio by a Monte Carlo–based particle injection technique. Particles are injected at random locations in a small region near the L1 point. In the original code, the region is a box located on the primary side of the L1 point, and the L1 point is at the center of one face. Particles are injected with velocity vectors that are calculated under the assumption of sound speed flow through the L1 point, and we naturally recover the trajectories of Lubow & Shu (1975). In order to resolve the accretion spot, we used an effective scaled particle size of 10 km, or $h \sim 10^{-4}$ in simulation units, where the stellar separation $a \equiv 1$. With particles this small, we found that the particle trajectories were ballistic and not behaving as a fluid (cf. Cash 2002, 2004). The solution we arrived at was to move the injection region to the *secondary* side of the L1 point and to implement a reflecting boundary plane approximately $30h$ from the L1 point. We inject particles with zero velocity in this region

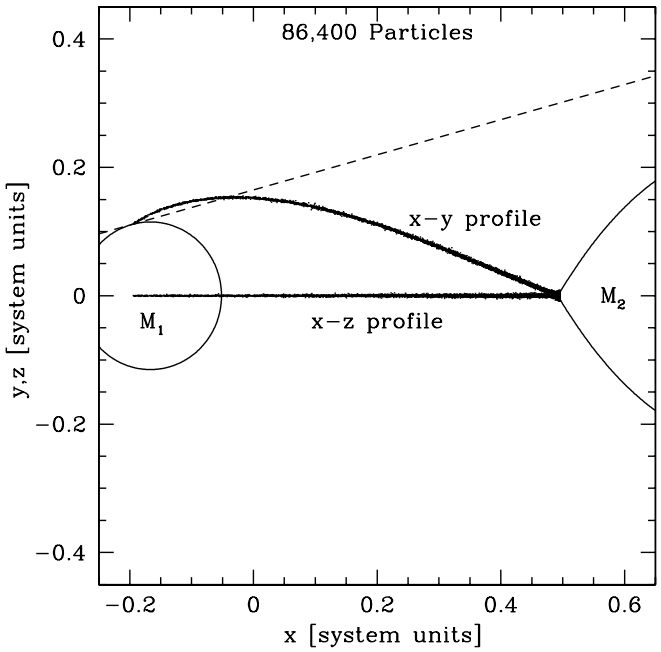

FIG. 1.— Stream profiles in the planes parallel and perpendicular to the orbital (x-y) plane. Also, the horizon of the impact spot is shown as the dashed line. Note that the altitude of the incoming accretion stream at the white dwarf surface is $\lesssim 20^\circ$ above the local horizon.

and hence create a crude pressure-supported atmosphere that naturally leads to a physical flow distribution through the L1 region into the Roche potential of the primary. To avoid spuriously generated sound waves when injecting particles, we find that preferentially injecting particles near the base of the atmosphere, where the density is significantly higher, is an effective technique, since viscous interactions tend to quickly damp any excited modes. This technique provides the most accurate flow dynamics through the L1 region obtainable within the SPH approach.

The Reynolds number is defined as

$$\mathrm{Re} = \frac{v_s L}{\nu}, \tag{1}$$

where v_s is the mean fluid velocity, L is the characteristic size of the region, and ν is the dynamic fluid viscosity. We can estimate the Reynolds number in the L1 region in our simulation by using the results of Monaghan (1997), who finds that the kinematic shear viscosity within the SPH formalism can be approximated as

$$\nu = \frac{15}{112} K v_{\mathrm{sig}} h, \tag{2}$$

where K is a constant ($K \sim 0.5$) and $v_{\mathrm{sig}} = c_i + c_j$ is the signal velocity between particles i and j. As noted above, we place our reflecting surface $30h$ behind the mathematical L1 point, which is roughly the width of the stream at the L1 point (see Fig. 1), and we use this as the characteristic size L (in pipe flow, the width of the pipe is taken as L). The mean fluid velocity is $v_s \sim 0$ at the reflecting wall and $v_s \sim c_s$ as the flow passes through the L1 point, so we use $v_s = c_s/2$ in the estimate of the Reynolds number. Then, from equations (1) and (2) and using $K \sim 1/2$, $v_{\mathrm{sig}} = c_i + c_i \sim 2c_s$, and $L \sim 30h$, we have

$$\mathrm{Re} = \frac{v_s L}{\nu} \sim \frac{(c_s/2)(30h)}{(15/112)(1/2)(2c_s)h} \sim 112. \tag{3}$$

This value of the Reynolds number is roughly 3–4 orders of magnitude lower than that at the typical transition to turbulent flow, so we expect the fluid near the L1 region to be nonturbulent. Furthermore, we note that Deloye et al. (2007), in their recent study of the structure and evolution of mass-donating secondary stars, found that the atmospheric structure of these stars just after mass transfer is initiated is characterized by radiative stability at the photosphere, a thin and weak subphotospheric convection zone, and then another radiative zone that extends to the core.

As discussed above, particles that are accreted onto the primary are immediately reinjected in the L1 region, so that a constant number of particles is maintained in the simulation and a dynamical equilibrium flow is established. For the simulation presented here, a steady-state mass transfer rate is established less than one orbit after the number of particles reaches its preset maximum value.

2.2. *The Model*

For the current study, we adopt the system parameters suggested by Marsh & Steeghs (2002) for V407 Vul: $P_{\rm orb} = 9.5$ minutes, $M_1 = 0.5\ M_\odot$, $M_2 = 0.1\ M_\odot$, and $R_1 = 0.0144\ R_\odot$. The orbital separation is calculated from Kepler's third law and is taken to be constant. Distances are scaled so that the orbital separation is unity in dimensionless system units. Because the mass of the SPH particles formally drops out of the equations (see Simpson & Wood 1998), no particular mass transfer rate is assumed a priori. The total number of particles is set to 86,400. Particles are given an initial temperature of 20,000 K, as is appropriate for the heated face of the donor star (Marsh & Steeghs 2002). The viscosity coefficients for the Lattanzio et al. (1986) artificial viscosity prescription are $\alpha = 1.0$ and $\beta = 0.5$, although viscosity is expected to play a negligible role in the dynamics of a stream of plasma in free-fall. An ideal equation of state is used, with $\gamma = 1.01$. The smoothing length was set to a value expected to be small with respect to the impact spot, which in our case was $h = 1.1493 \times 10^{-4}$ in simulation units, or $h \approx 10$ km. Tests were done with slightly larger values of h and the result did not change significantly. With a smoothing length of this size, we were forced to use 6000 time steps per orbit with three levels of refinement (i.e., $\delta t_0 = P_{\rm orb}/6000$, $\delta t_1 = \delta t_0/2$, or $\delta t_2 = \delta t_0/4$), as is described more fully in Simpson & Wood (1998). We note that the time of flight t_f from the L1 point to impact can be estimated using Kepler's third law with $a' \sim a/2$, and then the time of flight from the L1 point to impact is roughly $t_f \sim (1/2)(a'/a)^{3/2} P_{\rm orb} \sim P_{\rm orb}/5 \sim 1$–2 minutes, where the factor of 1/2 is the result of the particle completing only half the orbit.

While we make an attempt to accurately calculate the stream profile from the L1 region to the impact spot, we make several simplifying assumptions. First, we assume that the rotation of the secondary and the surface flow on the secondary star are negligible. This is likely to be a reasonable assumption, as the secondary is almost certainly corotating at the binary period. We further assume for the purposes of these calculations that in the absence of magnetic fields, the accretion spot size will not be greatly enhanced by interactions with the fluid already at the impact point, and we assume that each particle impacts at the point where its trajectory takes it through the radius of the primary. This assumption should hold to a good approximation, because the fluid in the accretion stream is highly supersonic when it impacts the surface, and in the absence of significant surface magnetic fields, the surface fluid is unable to apply any force on the incoming fluid before impact, with the exception of the (negligible) radiation pressure. Finally, in all calculations, radiative effects and magnetic forces are explicitly ignored.

2.3. *Analysis*

As described above, our technique lends itself to examining the cumulative distribution of particles over a long span of simulation time. Once our simulations have reached dynamical equilibrium, the probability distribution function of the particles is constant with time. By utilizing a Monte Carlo approach to particle injection, we ensure that the particular positions of the particles change over the course of the simulation. We further ensure a random selection of particles by sampling the simulation every 60th time step, so that a particular particle does not contribute to the number density of particles in any location more than once. Note that particles within the Roche lobe of the secondary could potentially be sampled many times by this technique, but this is of no concern here. With these aspects in mind, a two-dimensional Eulerian mesh (with small thickness) is created that slices through a region of interest, and the number of particles that lie within each grid zone is summed over all of the time steps included by the above criterion. In this way, we effectively increase the resolution of our results and reduce the noise inherent to the SPH technique (see also Wood et al. 2005).

Many of the above ideas are applicable to the characterization of the impact spot. The key difference is that we record the impact position of every particle accreted, as opposed to sampling every 60th time step. This is because each particle can only cross the surface of the primary one time by design, and so the Monte Carlo procedure for particle injection, coupled with the significant mixing within the Roche lobe of the secondary, serves to randomize the particle impact points. Also, since the impact spot lies on the curved surface of the primary, we lay our mesh on this curved surface and utilize the angular position of the impacts to bin them into grid zones. While this creates zones of different linear dimensions, the effect is negligible, since the impact spot lies in a very small region centered on the orbital plane. Once the particles have been binned, the relative positions of the grid zones are converted back to linear dimensions, so the distances presented below are actually arc lengths. With this complete, we fit the distribution with a bivariate Gaussian, using a nonlinear least-squares analysis.

3. STREAM CHARACTERISTICS

In this section, we briefly recount the results of several previous studies that explored the dynamics of the mass transfer stream in accreting binary stars. We focus on two regions, namely, the L1 region and the impact spot on the primary, the former primarily for validation of our technique.

3.1. *The L1 Region*

In the L1 region, Lubow & Shu (1975, 1976) showed via semianalytic methods that the density cross section of the stream should be Gaussian and decrease in overall density as r^{-1}, where r is the distance from the L1 point along the center of the stream. They also showed that the stream is deflected by an angle of $\theta \approx 20.8^\circ$ from the line connecting the centers of the stars (for a mass ratio of $q = 0.2$). Later numerical work by Oka et al. (2002), which accounted for the surface flow on the secondary, found that the stream was approximately Gaussian about its center (slightly bow-shaped, convex toward the trailing side), decreased as $r^{-0.8}$, and had a deflection angle that was smaller by roughly a factor of 2 compared to that of Lubow & Shu.

3.2. *The Accretion Stream Impact Region*

As the stream material accelerates toward the primary, it is stretched by tidal forces that act to narrow the stream, especially

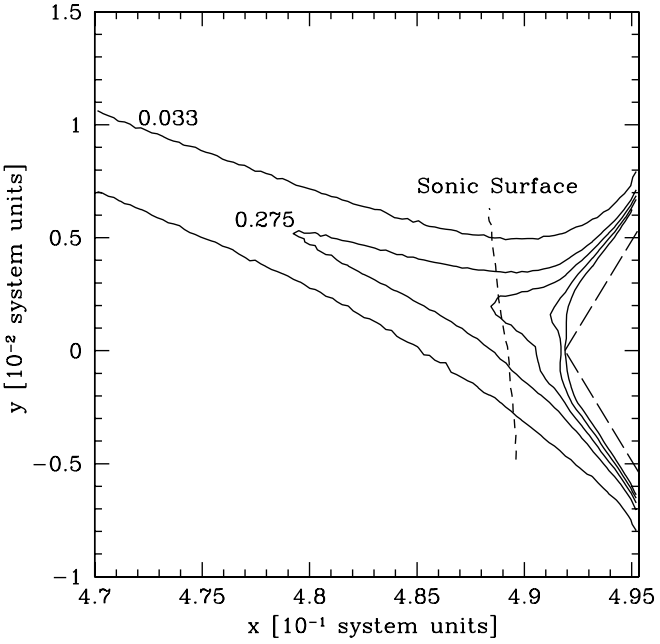

FIG. 2.—Equidensity contours in the L1 region. The density is normalized to unity on the contour that crosses over the L1 point. Note the different scales on each axis.

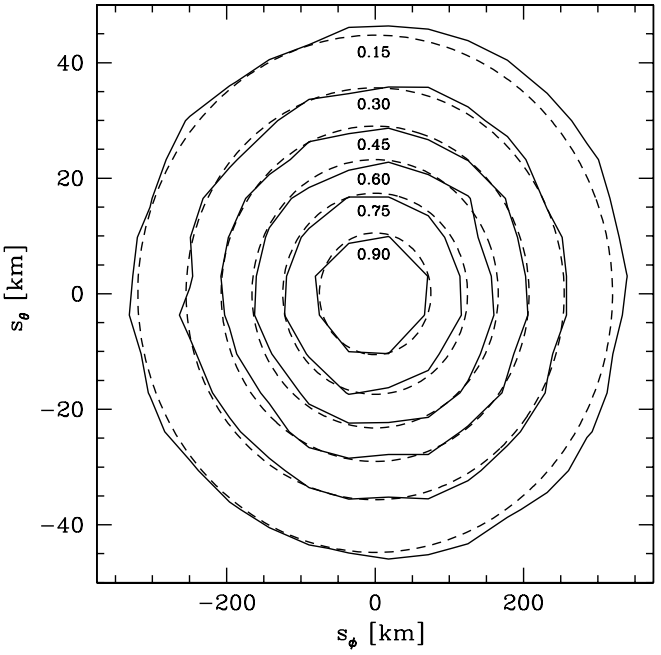

FIG. 3.—Contours of constant mass flux at the impact spot. The origin is set to the center of the fitted distribution (*dashed lines*). The values shown have been normalized to unity at the central maximum value. Note the different scales on each axis.

in the z-direction. This was predicted by Lubow & Shu (1976), who showed that the vertical stream width at closest approach to the primary should be of order the hydrostatic scale height of a disk at that same radius. The pressure scale height of a hydrostatic disk at $r = R_1$ from the center of the primary is approximately given by

$$H_p \sim \left(\frac{kTR_1^3}{GM_1 m_p}\right) \sim 6 \times 10^{-4}$$

in simulation units. Lubow & Shu (1975) find that the stream width in the orbital plane should be roughly a factor of 5 larger than the vertical width at closest approach, or $\sim 3 \times 10^{-3}$ in simulation units. While in our case the stream is intercepted by the surface of the primary before it reaches its closest approach, we take these values as approximate, and we indeed find our results to be in good agreement with those of Lubow & Shu (1975, 1976).

4. RESULTS

In Figure 1, we show the trajectory of the stream by plotting the stars and the SPH particles, viewed at orientations perpendicular and parallel to the orbital plane, at a single time step. As previously noted, the impact spot on the primary white dwarf is on the far side as viewed from the secondary (Marsh & Steeghs 2002).

As a proof of concept, we begin by analyzing our results for the flow in the L1 region. Our results are shown in Figure 2 as density contours of a slice centered on the orbital plane. We find that the stream is indeed approximately Gaussian-distributed about its center line, decreases in density as approximately $r^{-0.5}$, and is deflected by an angle of $\theta \approx 21^\circ$, in reasonable agreement with the Lubow & Shu (1975, 1976) results.

In Figure 3, we show contours of constant mass flux through the surface of the primary and the best fit obtained via nonlinear least-squares analysis using a bivariate Gaussian function. For the purposes of fitting, a coordinate system with the origin at the center of the mass flux is employed. The mass flux, Φ, found by our model is of the form

$$\Phi(s_\phi, s_\theta) = N_\Phi \exp\left[-\frac{1}{2}\left(\frac{s_\phi^2}{\sigma_\phi^2} + \frac{s_\theta^2}{\sigma_\theta^2}\right)\right], \qquad (4)$$

where N_Φ is a constant scaling factor, $s_\phi = \phi R_1$ is the arc length in the azimuthal direction, $s_\theta = \theta R_1$ is the arc length in the polar direction, and σ_ϕ and σ_θ are the standard deviations in these directions. In these coordinates, s_ϕ increases in the $-x$ direction and s_θ increases in the $+z$ direction. The result shown in Figure 3 is normalized to unity at the origin. The best-fit model gives $\sigma_\phi = 0.0019$ and $\sigma_\theta = 0.00026$ in simulation units, or $\sigma_\phi = 164$ km and $\sigma_\theta = 23$ km in physical units. The eccentricity of the resulting ellipse is $e = \left[1 - (\sigma_\theta/\sigma_\phi)^2\right]^{1/2} \approx 0.99$.

5. DISCUSSION

Looking again at Figure 1, it is apparent that the supersonic accretion stream impacts the white dwarf surface with a nearly horizontal trajectory. The altitude angle of the stream as viewed from the impact point is $\lesssim 20^\circ$. A very approximate mental picture of the situation can be achieved by considering a narrow, high-velocity jet of water impacting the surface of a pool with a similarly shallow altitude angle, and in fact the experiment is so easily available that we recommend the interested reader actually try it. In the stellar case, the shock-heated surface fluid will be promptly carried away from the impact point, and the accretion stream will always be impacting fresh material that is entrained from the surrounding $T \sim T_{\rm eff}$ atmosphere. There will be strong radial flows toward the core of the impact spot, which will serve to advect on a somewhat slower timescale the specific kinetic energy of the accreting material in the lower density outer volume of the stream.

We characterize the shape of the impact region as an "$N\,\sigma$" ellipse ($N \in \mathbb{R}$), with semimajor and semiminor axes given by,

for example, $a = \sigma_\phi$ and $b = \sigma_\theta$ for the 1 σ case. If we now assume that our coordinate system is centered on the centroid of the mass-flux distribution and that the distributions along both the ϕ- and θ-axes are normal Gaussians, then the constraining equation for the bivariate normal density distribution for the $N\,\sigma$ contour is (for example, see § 4.2 of Kawka et al. 2004)

$$\left(\frac{s_\phi}{N\sigma_\phi}\right)^2 + \left(\frac{s_\theta}{N\sigma_\theta}\right)^2 < 1 \tag{5}$$

or

$$\left(\frac{s_\phi}{\sigma_\phi}\right)^2 + \left(\frac{s_\theta}{\sigma_\theta}\right)^2 < N^2. \tag{6}$$

The joint probability of finding an object within the $N\,\sigma$ ellipse is then the integral of the probability density function inside the ellipse:

$$P(N\ \sigma) = \frac{1}{2\pi}\int_{-N}^{N} e^{-u^2/2} \int_{-\sqrt{N^2-u^2}}^{\sqrt{N^2-u^2}} e^{-v^2/2}\, dv\, du, \tag{7}$$

where $u = s_\phi/\sigma_\phi$ and $v = s_\theta/\sigma_\theta$. This yields, for the 1, 2, and 3 σ contours,

$$P(1\ \sigma) = 0.36, \tag{8}$$

$$P(2\ \sigma) = 0.86, \tag{9}$$

$$P(3\ \sigma) = 0.99. \tag{10}$$

Thus, approximately 86% of the mass in the accretion stream impacts a spot of area $A_{2\,\sigma} = 47,400$ km^2, or roughly a fraction of $f_{2\,\sigma} = 3.8 \times 10^{-5}$. The 3 σ profile (99% of the mass flux) yields an area of $A_{3\,\sigma} = 107,000$ km^2, or roughly a fraction of $f_{3\,\sigma} = 8.5 \times 10^{-5}$, or about the size of Iceland on a white dwarf of radius $\sim 1.5\ R_\oplus$. Our numerical results confirm that the footprint of the accretion stream is remarkably compact, which is consistent with the requirement of the DI model that we set out to test.

We can determine whether the accretion stream penetrates below the photosphere by comparing the ram pressure of the accretion stream to the gas pressure in the white dwarf atmosphere. If we take a conservative estimate for the accretion rate of $\dot{M} = 10^{-10}\ M_\odot$ yr^{-1} (Deloye et al. 2007), then we find that the distribution of the stream ram pressure in the radial direction has the same form as the mass flux given above, with a peak value of 3.4×10^9 dynes cm^{-2}, as is shown in Figure 4. White dwarf model atmosphere calculations (Vennes & Fontaine 1992; Kawka et al. 2007) for a $T_{\rm eff} \approx 20,000$ K, $\log g = 7.75$ white dwarf yield gas pressures at optical depths $\tau = 1$ and 10 of $P_{\rm gas} \approx 3 \times 10^5$ and 2×10^6 dynes cm^{-2}, respectively. Thus, $P_{\rm ram} \gg P_{\rm gas}$, and more than 99% of the mass flux should advect below the photosphere, where the bulk of its energy can be thermalized as in the blob accretion model proposed for some polars (Kuijpers & Pringle 1982; Frank et al. 1988; King 2000).

Marsh & Steeghs (2002) suggested that because the specific kinetic energy of the accretion stream enters at such a shallow angle to the surface, there should exist a high-luminosity region just downstream of the accretion impact point that emits in soft X-rays, and further downstream in the prograde equatorial flow, one would expect the spectral energy distribution to soften further toward the mean stellar effective temperature. Ramsay et al. (2005) report spectral softening as the flux declines toward the off phase in V407 Vul. The mean effective temperature of HM Cnc is estimated by Barros et al. (2007) to be in the range 18,500–32,400 K (and probably similar for V407 Vul, whose temperature is currently unmeasurable because of the G star that is coincident with that binary). We assume a value of $T_{\rm eff} \approx 25,000$ K for the purpose of some simple estimates discussed below. The peak optical radiation will thus lead the X-ray peak in orbital phase. Recent observations (Barros et al. 2007) indicate that both HM Cnc and V407 Vul are characterized by the optical pulses leading the X-ray pulses by about 0.2 in orbital phase, and that earlier claims (Israel et al. 2003, 2004) that the optical and X-ray pulses were antiphased were the result of incorrect timing corrections for the optical data.

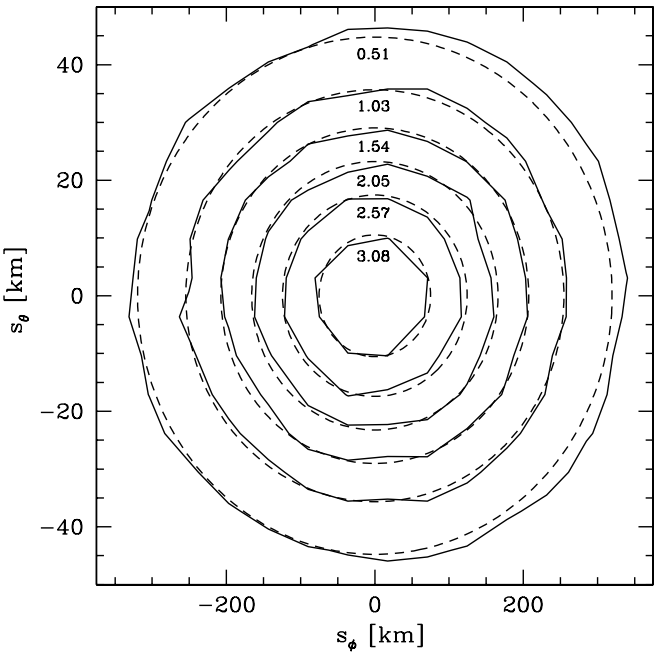

FIG. 4.—Contours of constant ram pressure in the radial direction at the impact spot. The values shown are in units of 10^9 dynes cm^{-2}.

We can crudely model the surface luminosity distribution using four zones: the first three are the accretion spot, the soft X-ray spot, and the optical spot, each of which is assumed to be uniformly illuminated, and the fourth is the remaining stellar photosphere. All three of the spots will be highly elongated features, and we approximate them very roughly as ellipses with a common focus (the center of the impact spot) and eccentricity[2] (see Fig. 5). As the newly accreted and shock-heated gas flows along the equator, shear mixing and high levels of turbulence will effectively spread the width of the accretion luminosity flow in latitude as the material propagates in longitude away from the impact spot.

Because the X-ray flux is observed for 60% of the orbital period, the soft X-ray–emitting region must have a linear extent of $\sim$10% of the circumference of the star, or equivalently 0.1 in orbital phase. This corresponds to a physical length of $s \approx 0.1(2\pi R_1) = 6100$ km, which is roughly 9 times longer than the full length of the 2 σ accretion spot discussed above. Measured from the center of the accretion spot, the distance to the

[2] We note that this approximation is simply the assumption that the area of the spots are proportional to the square of the length. The results would be essentially the same for scaled rectangular regions where all three aligned on one edge.

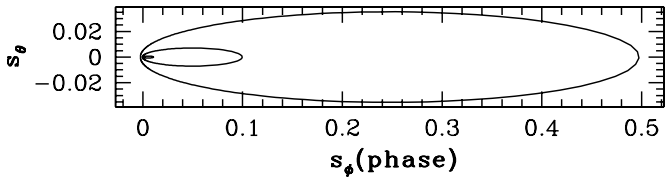

FIG. 5.—Schematic diagram of a crude three-zone model. Assuming that the impact spot, X-ray spot, and optical spot can all be characterized as uniformly illuminated ellipses with the same eccentricity ($e = 0.99$ is shown), and using the observational constraints, we find that the X-ray spot extends for roughly 0.1 in phase, while the optical spot would extend for ~0.5 in phase, or half the circumference of the primary white dwarf.

center of the X-ray spot will be roughly 0.05 in phase, or 3050 km. Because for high-eccentricity ellipses the distance from the focus to the center of the ellipse is $ea \approx a$, for a uniformly illuminated optical spot to lead the X-ray spot by 0.20 in phase, its center would have to be at a phase angle of 0.25 as measured from the accretion spot, which then implies that the optical spot extends for ~0.5 in phase around the primary white dwarf (Fig. 5). In the limit in which the area scales as the square of the ellipse length minus the area of the next smaller ellipse, the ratio of areas of the three zones is then 1 : 80 : 1920, and the ratio of the areas of the X-ray to optical spots is 1 : 24. In the limit in which the areas of the zones scale simply as the length of the zones (constant width of order the impact spot width), the ratio of areas for the three zones would be approximately 1 : 9 : 45. We note that the real emission regions will have monotonically decreasing radiation fluxes as a function of distance from the impact spot, which then means that the above estimates are lower limits to the linear extents of the X-ray and optical zones.

Barros et al. (2007) reports that the peak-to-peak amplitude for HM Cnc is roughly 25% in the optical. For a 2 σ spot viewed in the center of the stellar disk, this implies a spot temperature that is some 16% higher than that of the surrounding photosphere (~29,000 K). At an inclination of $i = 45^\circ$, the spot temperature needs to be some 40% higher than that of the surrounding photosphere (~35,000 K). The amplitudes in V407 Vul are diluted, and thus not known unambiguously, because of the G star that is along the same line of sight.

The DI model appears to be able to account for the observations of both the V407 Vul and HM Cnc systems, if we accept the results of Deloye & Taam (2006) and D'Antona et al. (2006), which state that a contracting lower mass secondary can yield a negative rate of period change and a steady accretion rate for a sufficient length of time that the objects' space density is high enough to be consistent with the observations. Cropper et al. (2004) suggests that the character of the X-ray light curves of these two systems is difficult to understand in the context of the DI model; they propose that within the DI model, one would expect an X-ray light curve that showed a slow rise to maximum and a steep decline, which is opposite to that observed. Ramsay et al. (2005) find that the spectral softness varies over the orbital phase and interpret this to mean that the X-ray–emitting region has some temperature structure. More work, both observational and theoretical, will be required in order to understand the nature of the luminosity distribution on the surface of the white dwarf primary within the DI model and to find out whether there is a unique solution that explains the set of observations.

6. CONCLUSIONS

We have shown that for the system parameters appropriate to V407 Vul, the impact spot size estimated with a hydrodynamics simulation is small enough to be consistent with the requirement of the DI model of Marsh & Steeghs (2002). In summary, we find:

1. The impact spot calculated for the system parameters of V407 Vul is very compact, with an effective area of only 47,400 km^2 or a fraction of $f = 3.8 \times 10^{-5}$ of that of the primary star, if we use the 2 σ contour through which 86% of the mass flows. The 3 σ profile (99% of the mass flux) encloses an area of $A_{3\,\sigma} = 107,000$ km^2, or roughly a fraction of $f_{3\,\sigma} = 8.5 \times 10^{-5}$ of the stellar surface area. The mass flux at the spot is characterized by a bivariate Gaussian distribution with standard deviations of $\sigma_\phi = 164$ km and $\sigma_\theta = 23$ km.

2. Within the DI model, the accretion stream impacts the surface nearly horizontally (with an altitude of $\lesssim 20^\circ$) and supersonically. The specific kinetic energy is advected and thermalized below the photosphere, to be reemitted downstream from the impact point in a very elongated region along the equator, and this equatorial flow is characterized by decreasing localized temperature and therefore decreasing spectral energy distribution.

3. The X-ray–emitting region must extend for ~10% of the equatorial circumference in order to account for the visibility of the X-ray source for ~60% of the orbit. This region then should be centered roughly on phase 0.05, measured along the equator from the impact point. In order for the optical phase to lead the X-ray phase by 0.2, the optical region should be centered at phase ~0.25, which then implies that the region has a full extent of ~0.5 in phase, or half or more of the circumference of the accreting white dwarf.

4. The fluid temperature must decrease from ~50 eV (~500,000 K) to ~25,000 K in the time it takes the equatorial flow to bring the newly accreted fluid roughly halfway around the primary. For a flow speed equal to the breakup velocity, this gives a time of 12 s and an exponential cooling timescale of ~4 s. For a more reasonable flow speed that is 1/10th of the breakup velocity, the cooling timescale is ~40 s. Note that in this context, "cooling" includes both radiative losses and entrainment of cooler gas from the surrounding photosphere.

Of the three viable candidate models for the observed systems V407 Vul and HM Cnc, the DI model appears to require the least number of "just so" parameter choices and to fit most easily the observational constraints. The major issue with the DI model is the observed negative rate of the period change, but as is discussed above, finite-temperature models of the secondary stars appropriate to these systems indicate overall contraction, which can yield stable mass transfer and a decaying orbit for a span of time sufficient to be consistent with the observed space density of the ultracompact AM CVn binaries (Deloye & Taam 2006; D'Antona et al. 2006). The polar model is then also not excluded by the observed dP/dt rates. Within the polar model, the accretion impact spot is likely to be located within $\pi/2$ radians from the stellar line of centers, and this makes the observed phasing problematic. The accretion stream trajectory in polars should be nearly vertical at impact, and because it is magnetically confined, there should be a standing shock. The absence of a hard component in the spectrum, as well as the absence of polarization, are further long-standing problems with this model (Cropper et al. 2004). The unipolar inductor model appears to be consistent with all of the observations, including the reported detection of radio emission (Ramsay et al. 2007), except for the relative phasing of the optical and X-ray light curves. In the UI model, the ~50 eV hot spots on the surface of the primary white dwarf are found along the meridian that passes through the line of centers, and the optical light curve results from the heated face of the secondary star. This model nicely fits the old, incorrectly time-calibrated

observations in which the optical and X-ray light curves were antiphased, but there appears to be no way for this model to explain the now currently accepted phase offset of 0.2 determined by Barros et al. (2007).

In future work, we plan to model the hydrodynamics of the impact region, using an implicit technique for estimating the radiation field and energy exchanges between SPH particles in the flux-limited diffusion approximation as described in Whitehouse et al. (2005), and to use simple ray-tracing concepts to estimate the emergent radiation as a function of inclination angle and orbital phase.

We thank Pasi Hakala for suggesting this project and Adela Kawka and Tom Marsh for useful discussions. We also thank the referee for suggestions that improved the presentation of the results. This work was supported in part by grant AST-0205902 to the Florida Institute of Technology.

REFERENCES

Barros, S. C. C., Marsh, T. R., Groot, P., Nelemans, G., Ramsay, G., Roelofs, G., Steeghs, D., & Wilms, J. 2005, MNRAS, 357, 1306
Barros, S. C. C., et al. 2007, MNRAS, 374, 1334
Beuermann, K., Thomas, H.-C., Reinsch, K., Schwope, A. D., Trümper, J., & Voges, W. 1999, A&A, 347, 47
Cash, J. L. 2002, Ph.D. thesis, Univ. Wyoming
———. 2004, in IAU Colloq. 190, Magnetic Cataclysmic Variables, ed. S. Vrielmann & M. Cropper (ASP Conf. Ser. 315; San Francisco: ASP), 272
Clarke, J. T., et al. 1996, Science, 274, 404
Cropper, M., Harrop-Allin, M. K., Mason, K. O., Mittaz, J. P. D., Potter, S. B., & Ramsay, G. 1998, MNRAS, 293, L57
Cropper, M., Ramsay, G., Wu, K., & Hakala, P. 2004, in IAU Colloq. 190, Magnetic Cataclysmic Variables, ed. S. Vrielmann & M. Cropper (ASP Conf. Ser. 315; San Francisco: ASP), 324
Dall'Osso, S., Israel, G. L., & Stella, L. 2006, A&A, 447, 785
———. 2007, A&A, 464, 417
D'Antona, F., Ventura, P., Burderi, L., & Teodorescu, A. 2006, ApJ, 653, 1429
Deloye, C. J., & Taam, R. E. 2006, ApJ, 649, L99
Deloye, C. J., Taam, R. E., Winisdoerffer, C., & Chabrier, G. 2007, MNRAS, 381, 525
Frank, J., King, A. R., & Lasota, J.-P. 1988, A&A, 193, 113
Goldreich, P., & Lynden-Bell, D. 1969, ApJ, 156, 59
Hakala, P., Ramsay, G., Wu, K., Hjalmarsdotter, L., Järvinen, S., Järvinen, A., & Cropper, M. 2003, MNRAS, 343, L10
Israel, G. L., Panzera, M. R., Campana, S., Lazzati, D., Covino, S., Tagliaferri, G., & Stella, L. 1999, A&A, 349, L1
Israel, G. L., et al. 2002, A&A, 386, L13
———. 2003, ApJ, 598, 492
———. 2004, Mem. Soc. Astron. Italiana Suppl., 5, 148
Kawka, A., Vennes, S., Schmidt, G. D., Wickramasinghe, D. T., & Koch, R. 2007, ApJ, 654, 499
Kawka, A., Vennes, S., & Thorstensen, J. R. 2004, AJ, 127, 1702
King, A. R. 2000, ApJ, 541, 306
Kuijpers, J., & Pringle, J. E. 1982, A&A, 114, L4
Lattanzio, J. C., Monaghan, J. J., Pongracic, H., & Schwarz, M. 1986, SIAM J. Sci. Stat. Comput., 7, 591
Lubow, S. H., & Shu, F. H. 1975, ApJ, 198, 383
———. 1976, ApJ, 207, L53
Lucy, L. B. 1977, AJ, 82, 1013
Marsh, T. R., & Nelemans, G. 2005, MNRAS, 363, 581
Marsh, T. R., & Steeghs, D. 2002, MNRAS, 331, L7
Monaghan, J. J. 1992, ARA&A, 30, 543
———. 1997, J. Comput. Phys., 136, 298
———. 2005, Rep. Prog. Phys., 68, 1703
Motch, C., & Haberl, F. 1995, in ASP Conf. Ser. 85, Cape Workshop on Magnetic Cataclysmic Variables, ed. D. A. H. Buckley & B. Warner (San Francisco: ASP), 109
Nelemans, G., Yungelson, L. R., Portegies Zwart, S. F., & Verbunt, F. 2001, A&A, 365, 491
Norton, A. J., Haswell, C., & Wynn, G. A. 2004, A&A, 419, 1025
Oka, K., Nagae, T., Matsuda, T., Fujiwara, H., & Boffin, H. M. J. 2002, A&A, 394, 115
Ramsay, G., Brocksopp, C., Wu, K., Slee, B., & Saxton, C. J. 2007, MNRAS, 382, 461
Ramsay, G., Cropper, M., & Hakala, P. 2006, MNRAS, 367, L62
Ramsay, G., Cropper, M., Wu, K., Mason, K. O., & Hakala, P. 2000, MNRAS, 311, 75
Ramsay, G., Hakala, P., Wu, K., Cropper, M., Mason, K. O., Córdova, F. A., & Priedhorsky, W. 2005, MNRAS, 357, 49
Ramsay, G., Wu, K., Cropper, M., Schmidt, G., Sekiguchi, K., Iwamuro, F., & Maihara, T. 2002, MNRAS, 333, 575
Simpson, J. C. 1995, ApJ, 448, 822
Simpson, J. C., & Wood, M. A. 1998, ApJ, 506, 360
Steeghs, D., Marsh, T. R., Barros, S. C. C., Nelemans, G., Groot, P. J., Roelofs, G. H. A., Ramsay, G., & Cropper, M. 2006, ApJ, 649, 382
Strohmayer, T. E. 2002, ApJ, 581, 577
———. 2004, ApJ, 610, 416
Vennes, S., & Fontaine, G. 1992, ApJ, 401, 288
Warner, B., & Woudt, P. A. 2002, PASP, 114, 129
Whitehouse, S. C., Bate, M. R., & Monaghan, J. J. 2005, MNRAS, 364, 1367
Wood, M. A., & Burke, C. J. 2007, ApJ, 661, 1042
Wood, M. A., Dolence, J., & Simpson, J. C. 2006, PASP, 118, 442
Wood, M. A., et al. 2005, ApJ, 634, 570
Wu, K., Cropper, M., Ramsay, G., & Sekiguchi, K. 2002, MNRAS, 331, 221